Development of a Fit-to-Surface and Lightweight Magnetic Coupler for Autonomous Underwater Vehicle Wireless Charging Systems

Chunwei Cai, Shuai Wu, Zhipeng Zhang, Longyun Jiang, and Shiyan Yang

***Abstract*—A novel magnetic coupler (MC) with cross-coupling mode is proposed in this article, which has merits of fit-to-surface and lightweight in receiver, and supports stable and efficient charging for autonomous underwater vehicles (AUVs). The proposed magnetic structure employing an arc bipolar transmitter and a compact dipole-coil-based receiver utilizes horizontal flux to establish strong and stable coupling against three-dimensional misalignment; the MC structure is constructed and optimized according to the magnetic field distribution characteristics. The influence of geometric parameters on the MC's performance is obtained based on ANSYS Maxwell simulation, with which the parameters of MC are optimized. In order to fully verify the performance of the designed MC, an AUV wireless charging system circuit is also developed. A wireless charging system prototype is built and tested with a 600 g receiver, and it can deliver 1 kW at a dc-to-dc efficiency of 95.1%. The experimental results under various operating conditions indicate that the proposed MC is viable and can be used for charging the AUVs.**

***Index Terms*—Autonomous underwater vehicle (AUV), magnetic coupler (MC), wireless charging.**

I. Introduction

AUTONOMOUS underwater vehicles (AUVs) play an indispensable role in ocean resources exploration, marine homeland security inspection, and so on [1]–[4]. However, the limited endurance and restricted cruising range have become the bottlenecks in the wide application of the AUVs [5]. The traditional way of wired recharging or battery swapping is complicated and time-consuming, resulting in the inflexibility of the AUV [6], [7].

Manuscript received November 17, 2020; revised January 29, 2021; accepted March 3, 2021. Date of publication March 8, 2021; date of current version June 1, 2021. This work was supported by the Natural Science Foundation in Shandong Province of China under Grant ZR2019MEE052. Recommended for publication by Associate Editor T. Mishima. (*Corresponding author: Chunwei Cai.*)

Chunwei Cai, Zhipeng Zhang, and Longyun Jiang are with the School of New Energy, Harbin Institute of Technology-Weihai, Weihai 264209, China (e-mail: caichunwei @hit.edu.cn; 18332550740@163.com; wfjianglongyun@163.com).

Shuai Wu is with the School of New Energy, Harbin Institute of Technology-Weihai, Weihai 264209, China, and also with the School of Electrical Engineering and Automation, Harbin Institute of Technology, Harbin 150001, China (e-mail: wushuai013@163.com).

Shiyan Yang is with the School of Electrical Engineering and Automation, Harbin Institute of Technology, Harbin 150001, China (e-mail: syyang@hit.edu.cn).

Color versions of one or more figures in this article are available at https://doi.org/10.1109/TPEL.2021.3064411.

Digital Object Identifier 10.1109/TPEL.2021.3064411

Wireless charging technology has spawned many applications including automatic guided vehicles [8], electric vehicles [9], [10], unmanned aerial vehicles [11], and AUVs [5], [12]–[20]. Compared to the wired charging technology, wireless charging system is more reliable and easier to automate the charging progress, since there are no physical connections. The convenience of the self-charging for AUVs is an important step to promote the further development of AUVs. This will greatly simplify the charging process and effectively expand the operation range of AUVs. So, the wireless charging is one of the key technologies to extend the cruising range of the AUVs.

A typical wireless charging system for the AUVs can be divided into three main components: power supply, magnetic coupler (MC), and pick-up. The MC is the core component of a wireless charging system that directly determines the magnetic field patterns and link's performance. Magnetic design is extremely relevant to the application abject. In the past, numerous special MCs have been proposed for the AUV wireless charging [5], [12]–[20]. Among them, cone type, ε type, curly coil structure, coaxial ring type, and three-phase ring type are several typical geometries of MC. A cone-type MC, which sets the elevation angle of the transmitting coil and the receiving coil at 45°, is proposed in [12]. The coupling coefficient of the cone-type MC can reach 0.78 when the gap is 5 mm, resulting in excellent power transmission capability and high efficiency. In this article, the gap refers to the distance between receiver and transmitter, and the intermediate medium in the gap is seawater rather than air. Unfortunately, as there is a convex in the receiver, it will change the original arc outward appearance of AUV's hull. As a result, the water flow resistance increases, and the mission time would be shorted accordingly. The pot-type MC, published in [13], has the same flux pattern compared to a cone type. It is much easier to be built since the standard pot magnetic core can be used to make a pot-type MC. But it suffers from the same complication that the AUV shape requires major modifications to obtain optimal performance. Recent studies focus on the development of MC that closely fits the AUV special arc surface. In [14], the standard E-core is modified to obtain an ε-type MC, and in [15], the traditional DD pad is converted to a curly coil structure. Since they all have an arc surface, the transmitter and receiver can closely attach to inner and outer arc surfaces of AUV, respectively. However, the coupling coefficient of ε-type MC is changing drastically for misalignment, leading to power controller design

difficultly. The curly coil structure has the advantages of strong tolerance to rolling misalignment and small size, but it will bear huge pressure inside the AUV shell due to the pressure of seawater, which may change the parameters of MC in underwater environment [21]. A coaxial ring-type MC, reported in [16], commits to improving the rotational robustness, in which the coaxial coil and ferrite core fitted with AUV's arc hull are adopted in the transmitter and the receiver, respectively. Since the throw flux by the transmitter is evenly distributed around the AUV's hull, the self-inductance and mutual-inductance are almost unaffected by the rotation misalignment. Further research by Kan *et al.* [5] indicated that there is a strong leakage magnetic flux inside the AUV. To address this problem, Kan *et al.* [5] proposed a three-phase segmented ring MC, in which the ring-type magnetic core of receiver was segmented to three parts and there are three transmitters correspondingly. The research revealed that the magnetic flux was converged in the area near the AUV shell, and there was no magnetic leakage interference in the center of AUV. However, the ring-type MC will use a large amount of ferrite core when it is applied to a large diameter AUV, which will increase the AUV's weight too much. Consequently, it is still a challenge in designing an MC when all the four aspects are considered, which are no change to AUV arc hull shape, low weight, small operation space of magnetic flux, and robust to misalignment.

As a candidate of AUV wireless charging, a novel magnetic structure is proposed with a comprehensive consideration of the four aforementioned performance aspects: weight of receiver, leakage magnetic flux, adaptability to AUV arc hull shape, tolerance to misalignment. And then, the influence of geometric parameters on the MC's performance is obtained based on ANSYS Maxwell simulation, with which the parameters of MC are optimized. To further verify the performance of the proposed MC, a wireless charging circuit and prototype design are detailed for AUV application. The validity of the proposal is also verified by simulations and experiments.

II. Analysis and Design of the Proposed MC

A. MC Design Fundaments

Coupling coefficient k is the most important parameter of an MC, since increasing k is the best approach for system performance improvement as output power can be improved as square of k, and it can also effectively increase the link efficiency [22]. The realization of the good power transfer performance for a wireless charging system requires not only good coupling capability but also high tolerance to the misalignment. The general AUV is an underactuated system, so AUV is not convenient for fine position adjustments after driving into the dock station, it is difficult to achieve precise alignment of the receiver to transmitter every time. Once misalignment occurs, the variations of magnetic parameters will constantly exist, which will reduce the system output capacity. The leakage magnetic flux does not directly contribute to the performance of the power transfer, but it inevitably appears in a wireless charging system. It is important to manage the leakage flux to prevent its adverse effect on an AUV's internal electronics devices. A good magnetic design is a compromise among all the aforementioned performance indicators. In summary, the MC design requirements for the AUV wireless charging are suggested as follows.

1) spare the change of the original arc shape of AUV's hull, which means that the transmitter and the receiver can fit to the surface of AUVs;
2) adequate tolerance capacity to the misalignment;
3) high coupling ability;
4) small magnetic field operating space and a lightweight receiver design;
5) simple structure and easy to install.

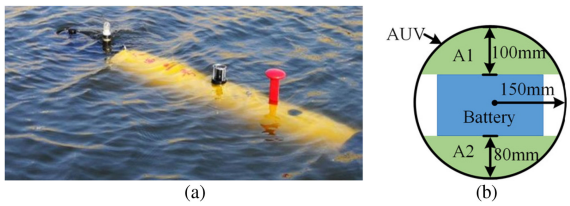

Fig. 1. (a) Photograph of the application object of the developed wireless charging system. (b) Axial section of the battery bunker of the AUV.

Magnetic design aims to fulfill the functional requirements of the application on an AUV. The receiver should be flexible to adapt to the AUV arc shape, compact to minimize the AUV space requirements, and easy to install. Nowadays, the emerging composite materials with the high specific strength and high specific modulus properties, such as fiberglass, are commonly used as the hull material for AUVs, which makes it possible to install the receiver in the AUV without affecting the original arc shape of the AUV's hull. According to the installation position of the receiver, it can be divided into installing the receiver outside the AUV shell, inside the shell (wrapped by the shell), and inside the AUV. If the receiver is installed outside the AUV, it will certainly increase the water resistance of AUV during navigation. If it is installed inside the AUV shell, it will increase the manufacturing difficulty of the AUV shell and reduce the mechanical strength of the shell. Installing the receiver inside the AUV will not increase the resistance of AUV operation, nor increase the difficulty of AUV manufacturing.

Usually, there are numerous precise sensors installed toward the head of the AUVs, the thrusters are placed at the tail, only the battery bunker in the middle of the AUV has space to install the pick-up. Fig. 1 shows the actual application object in this design and its axial section of the battery bunker, a cuboid lithium-battery is placed in the middle position, and two arc-shaped areas above (A1) and below (A2) the battery are available, and the upper area is expected to be filled with solid buoyant material. Therefore, this research concludes the placement of the receiver in the A2. In order to avoid adverse effects on the other existing electronics, the strong magnetic field operation space should be less than 80 mm.

B. Fundamental Flux Design

The role of a transmitter is to throw a desirable pattern of magnetic flux in a given space. Meanwhile, the receiver needs to capture the most magnetic flux around the transmitter it can. Therefore, the key in the design of an MC is the magnetic flux

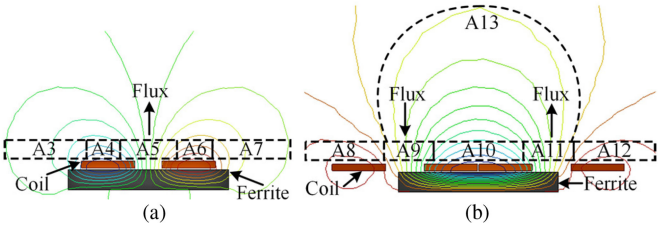

Fig. 2. Typical magnetic field type. (a) Nonpolarized. (b) Polarized.

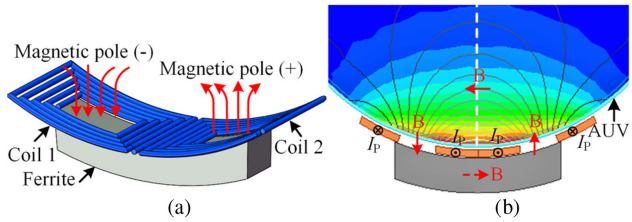

Fig. 3. Arc bipolar transmitter. (a) Geometry. (b) Magnetic field distribution by the ANASYS Maxwell.

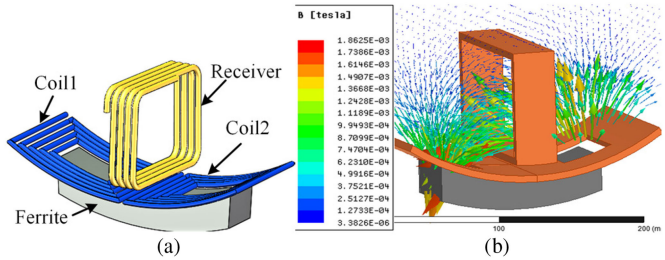

Fig. 4. Bipolar MC with air-core receiving coil. (a) Overall structure. (b) Magnetic flux distributions.

pattern design. The pattern of the fundamental flux depends even more on the geometry of coil and transmitter ferrite core. There are two typical types of transmitters [23], [24], nonpolarized and polarized, and their magnetic field shape is shown in Fig. 2. Polarized arc DD MC and nonpolarized arc circular MC have been tried to apply in AUV wireless charging by Ressurreição et al. [25] and Lin *et al.* [16], respectively.

Nonpolarized magnetic field [as shown in Fig. 2(a)] has only one magnetic pole at the center of a single coil. Its main magnetic flux is thrown from region A5 and returned by A3 and A7. To achieve magnetic coupling between transmitter and receiver, the receiving coil needs to enclose the flux in the A5. It should be noted that the return flux of A3 and A7 cannot be included in the receiving coil otherwise the thrown flux and the return flux will be offset. Therefore, the two sides of the receiving coil should be located in the A4 and A6, respectively. And then the main flux in the A5 can be exactly captured, henceforth the returned flux in the A3 and A7 will not have the offset effect. Polarized magnetic field [as shown in Fig. 2(b)] has two opposing magnetic poles at the center of two coils, so it can also be called a bipolar magnetic field. The main flux is thrown from A11 and returned from A9 after passing through A13. The flux counteraction problem caused by the reverse flux in A9 and A11 should also be avoided. In order to do this, the two sides of the receiving coil can be located in A10 and above A13, respectively, to capture the flux in A13.

On the premise of using the same ferrite core, the A10 is larger than the A4 (or A6) region. So, the bipolar coupling mode has a larger removable range for the receiving coil than the unipolar coupling mode. In addition, the A3 and A7 in the nonpolarized magnetic field are the returned regions of the main flux, and there are still strong magnetic fields in the two regions, which will generate strong leakage interference to the surroundings. The A8 and A12 in the bipolar magnetic field are the leakage flux regions, and no ferrite is used under them. Ferrite cores are used below the A13 of the main flux, so the reluctance of the main flux circuit is much smaller than that of the leakage flux circuit. As shown in Fig. 2(b), the magnetic fields in A8 and A10 are weak according to the density of magnetic lines. The bipolar coupling method has a better convergence effect on magnetic field and less magnetic leakage interference to the surroundings than the unipolar coupling method in the mall gap occasion. It can be seen that the bipolar coupled magnetic field has obvious advantages in reducing the misalignment sensitivity, improving the effective coupling flux, and reducing the leakage flux operating space. Therefore, the bipolar coupled magnetic field is chosen in this article.

Traditional bipolar transmitting pads are flat; there will be large gap when the plat transmitter is directly applied to the AUV with arc shape. The smaller the gap is, the stronger coupling ability, the better constrained magnetic leakage flux, and the smaller eddy current loss in seawater will be. Therefore, it is necessary to arc the traditional planar transmitter according to the actual shape of AUV. When arc the bipolar transmitter, two magnetic poles can be selected to be distributed along the AUV axis, or two magnetic poles can be selected to be distributed along the circumference of the shell of the AUV. This article chooses the latter scheme, as shown in Fig. 3(a). By doing so, the distance between the two magnetic poles can be appropriately shortened, and the magnetic flux density and coupling ability can be improved. The current direction of each coil is reversed, which leads to the reversed polarity of magnetic flux density B at each pole, as shown in Fig. 3(b). It can also be found that the main flux circulates in two adjacent magnetic poles and the flux is mainly distributed at the bottom of AUV hull, which can effectively reduce the operating magnetic field space of the wireless charging system.

Further analysis of the bipolar magnetic field is shown in Fig. 3(b). It is indicated that the main magnetic flux enters the AUV through one pole of transmitter, passes through the space bottom of the AUV, and then flow out from the other pole. The horizontal flux above the middle position of the transmitter [the dotted line position of Fig. 3(b)] is formed. If a vertical receiving coil is placed at the dotted line in Fig. 3(b), the thrown flux will be captured by the receiving coil. Therefore, the MC using cross-coupling mode shown in Fig. 4(a) can be developed. A finite-element simulation model is built to verify the capturing flux capability, as shown in Fig. 4(b); it is found that the flux

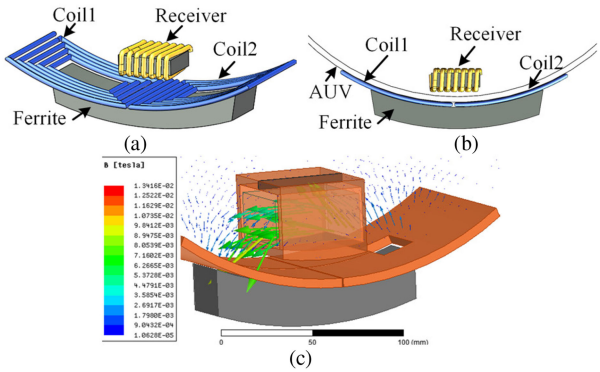

Fig. 5. Bipolar MC with guide ferrite core added at receiver. (a) Overall structure. (b) Axial view. (c) Magnetic flux distributions.

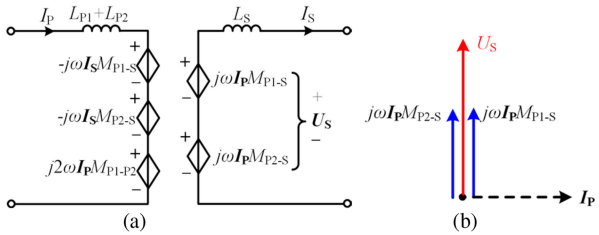

Fig. 6. (a) Equivalent circuit diagram of the proposed MC. (b) Induction voltage of the receiving coil from the two transmitting coils.

does pass through the receiving coil, and is also gathered near the AUV hull.

C. Reducing Receiver Volume by Adding Guide Ferrite

The AUV's internal space is extremely limited, which makes it an eternal pursuit for designers to compress the space occupied by the receiver as much as possible. Adding magnetic cores is an effective way to collect and guide magnetic flux toward the direction of expectation. Meanwhile, the density of copper is higher than that of ferrite; the use of ferrite on the receiver can reduce the copper consumption of coil with the same L_S. In order to further reduce the volume and magnetic field operating space of the receiver, a guiding ferrite core is added to the receiving coil, and the small volume MC is obtained as shown in Fig. 5. The receiver is equipped with a small I-type ferrite core, and the receiving coil is wound on the outer side of the core. Fig. 5(c) shows the magnetic flux vector of the MC after adding the core at the receiver. It can be seen that the main flux is guided by the core through the receiving coil, and the magnetic field operating space is effectively converged.

D. Transmission Characteristics Analysis

For further analysis of the proposed MC, the equivalent circuit is presented, as shown in Fig. 6, where the L_{Pi} ($i = 1, 2$) is self-inductance of the ith transmitting coil, L_S is self-inductance of the receiving coil, $M_{Pi\text{-}S}$ is mutual inductance between the ith transmitting coil and the receiving coil, $M_{P1\text{-}P2}$ is mutual inductance between the two transmitting coil, U_S is the inductive

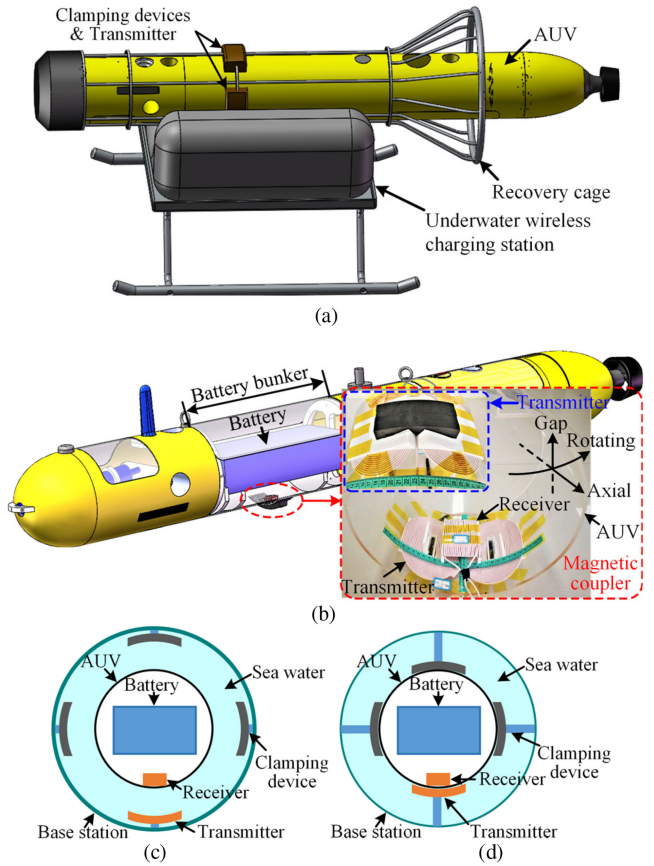

Fig. 7. (a) General overview of the AUV underwater docking station. (b) Proposed MC installed in the AUV body. Wireless charging base station at (c) noncharging state and (d) charging state.

voltage of the receiving coil, and I_P and I_S are the current flowing through the transmitting coil and the receiving coil, respectively. The advantage of the MC proposed in this article is that the magnetic flux emitted by any transmitting coil is mutually reinforcing to the receiving coil, and it is impossible to cancel each other. As shown in Fig. 6(b), if any transmitting coil has coupling with the receiving coil, the receiving coil will have induction voltage. Therefore, the developed MC has no dead point.

E. Overall Configuration

The overall configuration of the designed AUV underwater recharging station is shown in Fig. 7. During the charging process, the auxiliary clamping devices are extended to the AUV hull, which can well cope with the dynamic disturbance of water flow and effectively short the gap. The transmitter is embedded in one of the clamping devices to perform the charging task.

F. Interoperability Study of the Proposed MC

Considering the fact that there will be many AUVs with different diameters and power classes sharing one underwater charging station in the future, the interoperability of the transmitter for AUVs with different diameters and different power levels

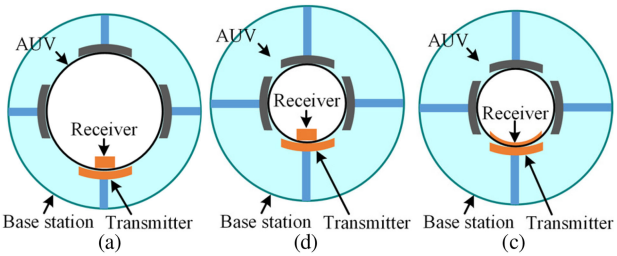

Fig. 8. Interoperability study of the MC with AUV with different diameters. (a) Proposed MC with large diameter AUV. (b) Proposed MC with small diameter AUV. (c) Face-to-face coil structure with small diameter AUV.

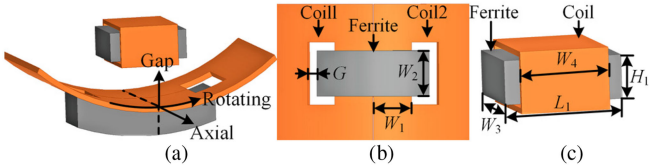

Fig. 9. MC. (a) Misalignment. (b) Design variables in transmitter. (c) Design variables in receiver.

TABLE I
PARAMETERS OF AUV HULL AND MISALIGNMENT RANGE

Parameters	Value
Diameter of AUV	300 mm
Thickness of AUV hull	4 mm
Rotational misalignment	[−10°, 10°]
Axial misalignment	[−30 mm, 30 mm]
Gap variation	[8 mm, 18 mm]

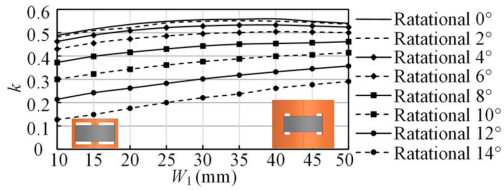

Fig. 10. k variation with W_1.

is also an important aspect to be considered. This part studies the interoperability of the MC for AUV of different diameters, and the power interoperability research will be carried out later.

In order to be compatible with AUV with different diameters, the transmitter needs to be designed according to the maximum diameter AUV. As shown in Fig. 8(a) and (b), with the same transmitter, the receiver of the proposed MC is placed at the bottom of the AUV and occupies a small radian, so the transmitter and receiver always ensure a small gap when used with AUVs of different diameters. However, in the traditional face-to-face coil structure [15], the gap will change greatly as shown in Fig. 8(c). Because the receiver of this proposal occupies a small arc of AUV, and the gap change caused by different AUV diameters is very small. Therefore, the proposal in this article has good performance in the compatibility of AUV with different diameters.

III. Practical Parameters Design of the Proposed MC

The magnetic structure can only roughly determine the flux pattern, and the excellent performance of the wireless charging system depends more on the optimal magnetic parameters. In this research, a three-dimensional finite-element analysis via ANSYS Maxwell is used to carry out the parameter design of the MC. The coupling coefficient, misalignment tolerance, and weight and volume are coupled with each other; the main objective of parameter design in this article is to balance those three performances.

A. MC Design Variables

When AUV homes and docks to recharging station, there will be inevitable rotational misalignment, axial misalignment, and gap variation [as shown in Fig. 9(a)]. AUV has the self-stabilizing mechanism, and the recharging docks are always located in the place where the ocean currents flow smoothly. So, AUV will only roll within a small angle. The AUV's hull parameters and the misalignment range that may occur during charging are summarized in Table I.

There are many variable parameters in the proposed MC; it is difficult to take all variables into account comprehensively. In this research, the size of the arc core at the transmitter is preliminarily determined by the requirements of rotational misalignment. The angle of 20° (rotational misalignment range) corresponds to the chord length of 52 mm. Besides, it is necessary to take the fact that the receiver has a certain length into consideration, and then the length, width, and thickness of the transmitting arc ferrite strip are set to be 118, 12, and 24 mm, respectively. The width of the transmitting core can be changed since multiple transmitting arc ferrite strips can be spliced together. Above all, the optimum design of the MC aims at seven parameters: the transmitting coil width W_1, gap G between transmitting coil and transmitting ferrite, transmitting core width W_2, receiving core thickness H_1, receiving core length L_1, receiving core width W_3, and receiving coil width W_4, as shown in Fig. 9.

B. Investigating Transmitting Coil Width W_1

The effect of W_1 on k with different rotational degrees is investigated; results are shown in Fig. 10. It shows that when the rotational degree is small (such as 0°–6°), k has extremum. When the rotational misalignment is greater than or equal to 8°, there is no extremum of k, and the curve shows an increasing trend. It should be noted that when the dislocation is no smaller than 8°, the slope of the corresponding curve increases gradually with the increase of the rotating degree, so increasing W_1 can reduce the change degree of the parameters caused by the dislocation. To ensure the charging reliability, 50 mm with low sensitivity to rotational misalignment is selected as W_1.

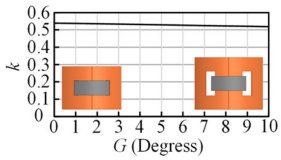

Fig. 11. k variation with G.

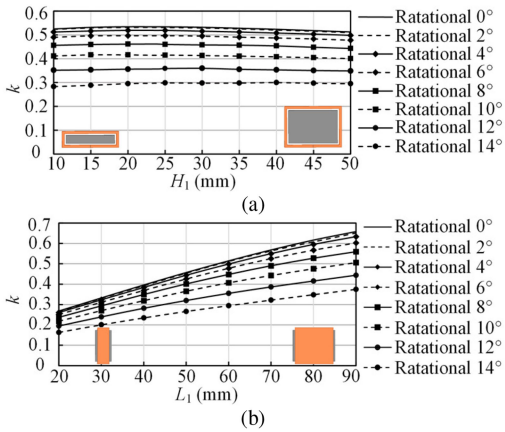

Fig. 12. k variation with (a) H_1 and (b) L_1.

C. Gap G Between Transmitting Coil and Transmitting Ferrite

The graph of Fig. 11 shows k variations as G increases. The k decreases gradually with the increase of G, but the reduction is small. If G is too small, the transmitting ferrite may not fit closely with the transmitting coil in actual MC development. Therefore, the G is set as 2° to simplify the installation task.

D. Ferrite Thickness H$_1$ and Length L$_1$ of Receiver

The graph of Fig. 12(a) shows k variations as H_1 increasing with different rotational misalignment. The extremum of each curve appears near H_1 equal to 20 mm. If H_1 is 10 mm, k will decrease by 0.24 when the rotational misalignment increases from 0° to 14°, and if H_1 is 50 mm, k will decrease by 0.22. The k drop caused by rotational misalignment is almost the same, which indicates that the sensitivity to rotational misalignment is almost independent of H_1. As the stronger coupling can lead to the high-power transmission efficiency, H_1 is set as 20 mm.

By changing L_1, the variation of the k is measured as shown in Fig. 12(b). It is shown that each curve has an increasing trend, that is, under the same rotational degree, the larger the L_1, the stronger the coupling ability. It can also discover that the slope of the curve decreases with the increase of the rotational degree, that is, increasing L_1 will boost the sensibility to rotational misalignment. When L_1 is 60 mm, k drops 0.1 as rotating 10°, and the fluctuation of the parameters of the MC is small. Therefore, L_1 is selected to be 60 mm.

In the above analysis, the parameters, mainly affecting sensitivity to rotational misalignment capability, have been determined. On the basis of the above parameters, the W_2 and W_3 together determine the tolerance capability to the axial misalignment. According to the requirements of axial misalignment and the design method of parameter scanning, the change rule of coupling parameters can also be found when W_2 and W_3 change, so as to complete the parameter optimization. Due to the limitation of page size, this part will not be repeated. Finally, W_2 is chosen as 48 mm and W_3 as 60 mm. The output voltage of the system is related to mutual inductance M and L_P, according to the following analysis results. In order to improve the output voltage level, the best way is to increase M without increasing the L_P, that is, to increase the receiver self-inductance L_S. Since the length and width of the receiving core have been determined, enhancing the L_S can only be achieved by increasing the number of receiving coil turns. There are two ways to increase the receiving coil turns in terms of increasing W_4 and adding winding layer of the coil. Adding the number of the winding layers will increase the gap between the transmitter and receiving core, which will reduce the coupling ability. Therefore, the way of winding a single-layer coil on the receiving core and covering all the receiving core with coil is chosen, which means that W_4 is set to 60 mm.

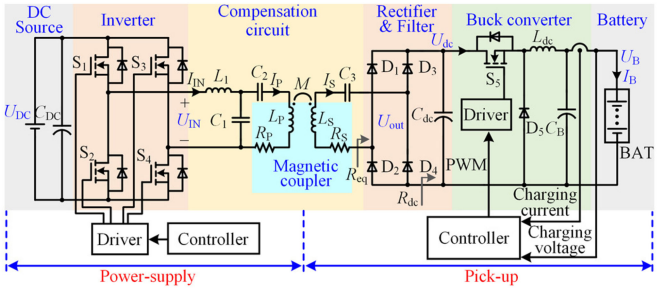

Fig. 13. Wireless charging system structure for AUVs.

IV. Circuit Development and Efficiency Improvement for the Best Performance of the Proposed MC

A. System Circuit Structure Development

In order to fully verify the performance of the designed MC, an AUV wireless charging system circuit is developed, as shown in Fig. 13; it consists of two independent parts named power supply and pick-up. U_{DC} is the dc power supply voltage. U_{IN} and I_{IN} are the output voltage and current of the inverter, respectively. U_{out} is the output voltage of the *LCC*-S resonant compensation network, and is also the input voltage of the rectifier. U_{dc} and I_{dc} are the voltage and current of the intermediate dc bus, respectively. U_B and I_B are the charge voltage and charge current, respectively. R_{eq} and R_{dc} are the equivalent resistances on the input and output sides of the rectifier, respectively.

In the power-supply side, a dc voltage source U_{DC} (100 V) is used to feed the whole system, and it is converted to 50 kHz ac voltage U_{IN} through the H-bridge inverter. The *LCC* compensation circuit is adopted in the power supply to produce a constant excitation current for the transmitter of the MC. Therefore, a near-constant magnetic field is generated.

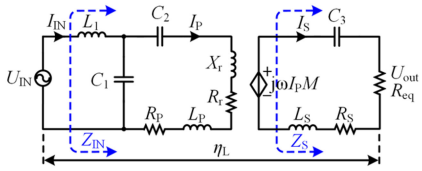

Fig. 14. Equivalent circuit of the wireless charging system.

Through the MC, energy is delivered from power-supply side to receiver via the magnetic field. On the pick-up side, series compensation is adopted. An H-bridge rectifier and capacitive filter are used to supply dc power to a buck converter. Then, the dc power is regulated by the buck converter to achieve CC/CV charging for the AUV battery.

B. Power Transfer Channel Output Voltage Deriving

Fundamental mode analysis is commonly used to analyze the resonant tank, in which only the fundamental harmonic is considered for simplicity. Since the series compensation is used at the pick-up, the input current of the rectifier is a sine ware, a capacitor filter is used to smooth the output current I_{dc} of the rectifier. According to papers [26] and [27], the equivalent resistance R_{eq} at the input side of the rectifier and output voltage of the rectifier are derived as

$$R_{eq} = \frac{8R_{dc}}{\pi^2} \tag{1}$$

$$U_{dc} = \frac{\sqrt{2}\pi U_{out}}{4}. \tag{2}$$

The inverter uses phase-shift modulation scheme, but its conduction angle is constant. The reason is that more power margin is reserved for the system to meet the demand of higher power. As mentioned in [23], the fundamental output voltage U_{IN} of the inverter is dependent on conduction angle Φ, defined as

$$U_{IN} = \frac{2\sqrt{2}}{\pi} U_{DC} \sin\left(\frac{\phi}{2}\right). \tag{3}$$

Then, the equivalent circuit model of the proposed wireless charging system can be obtained, as shown in Fig. 14. Here, Z_{IN} and Z_S represent the output impedance of the inverter and input impedance of the pick-up circuit, respectively. Z_r is reflection impedance, which represents the loading effect of the pick-up on the power supply. Ignoring the parasitic resistance of the coils, Z_{IN}, Z_S, and Z_r can be represented by the following:

$$Z_{IN} = j\omega L_1 + \frac{1}{j\omega C_1} // [j\omega(L_P - \frac{1}{\omega^2 C_2}) + (X_r + R_r)] \tag{4a}$$

$$Z_S = j\omega L_S + \frac{1}{j\omega C_S} + R_{eq} \quad Z_r = R_r + X_r = \frac{(\omega M)^2}{Z_S}. \tag{4b}$$

The excitation current of the transmitter can be given by

$$I_P = \frac{U_{IN}}{Z_{IN}} \frac{1/j\omega C_1}{(1/j\omega C_1) + j\omega[L_P - 1/(\omega^2 C_2)] + (X_r + R_r)}. \tag{5}$$

From Fig. 14 and (5), the output voltage of the *LCC*-S resonant channel at resonance condition can be represented by

$$U_{out} = \frac{j\omega M I_P}{j\omega L_S + 1/j\omega C_S + R_{eq}} = \frac{M U_{IN}}{L_P - 1/(\omega^2 C_2)}. \tag{6}$$

Combining (2), (3), and (6), the voltage of the intermediate dc bus becomes

$$U_{dc} = \frac{\sqrt{2}\pi}{4} \frac{M U_{IN}}{L_P - 1/(\omega^2 C_2)} \tag{7}$$

which represents the dc-to-dc steady-state transfer characteristic. The pick-up behaves like a voltage source and a dc–dc converter can be cascaded to the rectifier for regulating the current flowing to the battery.

C. System Parameters Design

According to Fig. 14, the system link efficiency of the proposed wireless charging system can be expressed as

$$\eta_L = \frac{R_r}{R_r + R_P} \frac{R_{eq}}{R_{eq} + R_S} = \frac{1}{1+1/a + (a+2+1/a)/(k^2 Q_{CP} Q_{CS})} \tag{8}$$

where "a" is a defined variable to simplify (8); Q_{CP} and Q_{CS} are the quality factors of the transmitting and receiving coils, respectively, and they can be expressed as

$$a = \frac{R_{eq}}{R_S}, \quad Q_{CP} = \frac{\omega L_P}{R_P}, \quad Q_{CS} = \frac{\omega L_S}{R_S}. \tag{9}$$

Then, by differentiating η_L with respect to a and equating the differential function to zero, the maximum link efficiency can be obtained as

$$\eta_{L-max} = \frac{k^2 Q_{CP} Q_{CS}}{\left(1 + \sqrt{1 + k^2 Q_{CP} Q_{CS}}\right)^2} \tag{10}$$

which is achieved at

$$a_{max} = \sqrt{1 + k^2 Q_{LP} Q_{LS}} \Rightarrow R_{eq-max} = R_S \sqrt{1 + k^2 Q_{LP} Q_{LS}}. \tag{11}$$

According to the relationship between R_{dc} and R_{eq} in (2), the optimum value of R_{dc} for maximum link efficiency can be obtained at $R_{dc-max} = \pi^2 R_S \sqrt{1 + k^2 Q_{LP} Q_{LS}}/8$.

The parameters of the MC measured by HIOKI LCR Meter are shown in Fig. 15. Combining the tested results of the MC, the value of $R_{dc\text{-}max}$ can be worked out, and it is 14.6 Ω.

As shown in Fig. 16, during the CC/CV charging process, the CC charging is used at the beginning until the charge voltage reaches the rated value. Then the charging mode switches to CV charging, and the charge current decreases accordingly. When the charge current is lower than the rated value, the charging process is completed. The equivalent load resistance of the

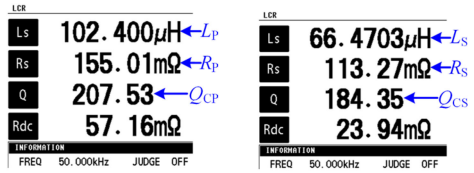

Fig. 15. Magnetic parameters of (a) transmitter and (b) receiver measured by LCR Meter.

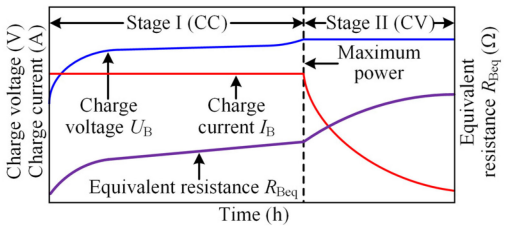

Fig. 16. Typical CC/CV charging characteristic of the Li-ion battery.

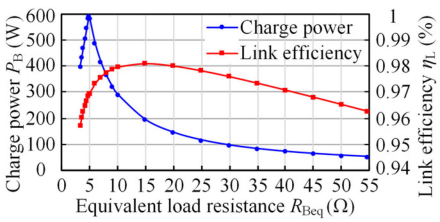

Fig. 17. Charge power and link efficiency vary with the load resistance.

charging battery R_{Beq}, which is defined as the ratio of charge voltage U_{B} to charge current I_{B}, increases with the charge time. In this article, an 11 A-CC/54 V-CV charging system is needed, in which the variation range of R_{Beq} is 3.3–4.9 Ω in CC stage and 4.9–54 Ω in CV stage. The maximum charging power point is at the switch point from CC to CV, and the R_{Beq} of the maximum power point is 4.9 Ω.

The variation of link efficiency η_{L} and charging power P_{B} with equivalent load resistance R_{Beq} in the charging process is shown in Fig. 17. It can be found that the high-power area does not coincide with the high efficiency area. When P_{B} is above 400 W, the range of R_{Beq} is 3.3–7.3 Ω, and the link efficiency is relatively low in this stage. A large amount of energy will be lost in the coupling channel and the complexity of the cooling system design will also be elevated.

In order to realize high-efficiency energy transmission of the wireless charging system, this article proposes a scheme to shift the link-efficiency curve to the left by using the impedance transformation ability of dc–dc converter [$R_{\mathrm{dc}} = \mathrm{f}(R_{\mathrm{Beq}}, D)$]; the schematic diagram of the efficiency optimization design is shown in Fig. 18. The D is the duty cycle of the dc–dc converter. By doing this, the high-power stage will coincide with the high-efficiency stage. As shown in Fig. 16, most time of the charging process is occupied by the high-power section during

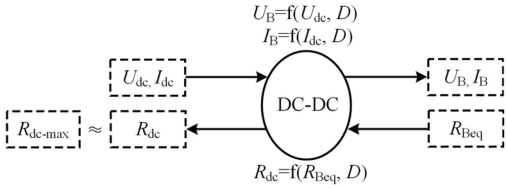

Fig. 18. Schematic diagram of efficiency optimization design.

TABLE II
OUTPUT CHARGE VOLTAGE AND INPUT RESISTANCE OF BASIC DC–DC CONVERTERS

Topology	Output voltage U_B	Input resistance R_{dc}	Input resistance range
Buck	DU_{dc}	R_{Beq}/D^2	R_{Beq} to $+\infty$
Boost	$U_{dc}/(1-D)$	$(1-D^2)R_{Beq}$	0 to R_{Beq}
Buck-Boost	$DU_{dc}/(1-D)$	$(1-D^2)R_{Beq}/D^2$	0 to $+\infty$

the charging process, and the change of resistance in the high-power section is very small. Therefore, through the efficiency optimization design, to adjust the R_{dc} of the high-power charging stage close to the $R_{\mathrm{dc\text{-}max}}$ is feasible and the loss in the whole charging process will be greatly reduced.

The impedance transformation function in Fig. 18 depends on the type of the dc–dc converters used. For example, in a buck converter, the output charge voltage U_{B} is

$$U_{\mathrm{B}} = DU_{\mathrm{dc}}. \tag{12}$$

Neglecting the power losses of the buck converter, the following equation is obtained:

$$\frac{U_{\mathrm{dc}}^2}{R_{\mathrm{dc}}} = \frac{U_{\mathrm{B}}^2}{R_{\mathrm{Beq}}}. \tag{13}$$

By incorporating (11) and (12), the input resistance of the buck converter can be obtained

$$R_{\mathrm{dc}} = \frac{R_{\mathrm{Beq}}}{D^2}. \tag{14}$$

Similarly, the output charge voltage and input resistance of any type of dc–dc converter can be obtained. Three typical dc–dc converter features are listed in Table II.

To move the efficiency curve to the left requires to adjust the R_{dc} to higher values than the R_{Beq}. The input resistance of the boost converter is limited to the range from 0 to R_{Beq}. The buck–boost converter increases the complexity of driver. Therefore, the buck converter is selected in this design.

By adjusting the duty cycle of the buck, the degree that the curve moves to the left can be controlled. In the above analysis, it is known that the charge power is the largest when the R_{Beq} is 4.9 Ω, the corresponding charging voltage U_{B} is 54 V, and the R_{dc} of the maximum link efficiency is 14.6 Ω. According to (14), the optimal duty cycle D of the buck circuit is 0.5795. Fig. 19 shows the change of charging power and link efficiency with R_{Beq} when the duty cycle D of buck converter in CV charging section is 0.5795. It has been considered that the duty cycle of CC charging stage cannot reach 0.5795. It can be found that

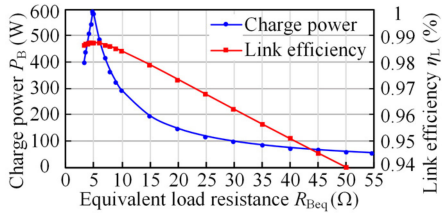

Fig. 19. Charge power and link efficiency vary with load resistance at $D = 0.579$.

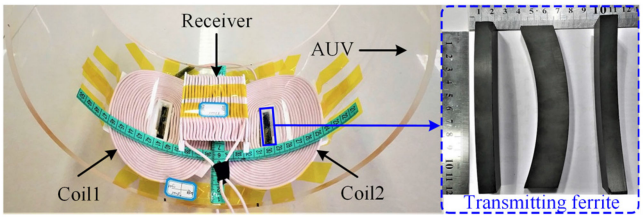

Fig. 20. Experimental models of the proposed MC.

the high charging power section of 400 W or above exactly corresponds to the high link-efficiency section. It is confirmed that the purpose of system efficiency optimization design is achieved by using this proposal, which means that in the process of CC/CV charging, the high-efficiency transmission is also ensured.

The MC misalignment causes the k reduction, which further affects the output voltage of the *LCC*-S wireless power supply network. If the voltage of the intermediate dc bus U_{dc} is set to 93.2 V (corresponding to $D = 0.579$) under the condition of precise alignment, the effect of system efficiency improvement is not obvious due to the misalignment in the actual underwater application. Therefore, it is necessary to consider the misalignment in advance when setting the U_{dc}. In Section V, it is found that the maximum drop of k is 23%. Considering that the system usually works in a small dislocation, on the basis of the ideal value of 93.2 V, the U_{dc} increases by about 20%, that is, the U_{dc} is designed to be 110 V. Eventually, the parameters of compensation elements can be determined based on (7) and resonance condition.

V. Simulations and Practical Validation

The influence of geometric parameters on the performance of the MC has been obtained in the above analysis, and the ideal parameters have been preliminarily selected. For practical validation of the proposal, prototypes of the proposed MC were manufactured as shown in Fig. 20. The prototype is only used as the structure description, and the actual test prototype also has a waterproof layer. Unfortunately, some ideal geometric parameters may not be realized in practice limited by existing standard ferrite strips, some of them are compromised according to the actual situation resulting in the parameters of the MC shown in Table III. The weight of the receiver in this design is 600 g.

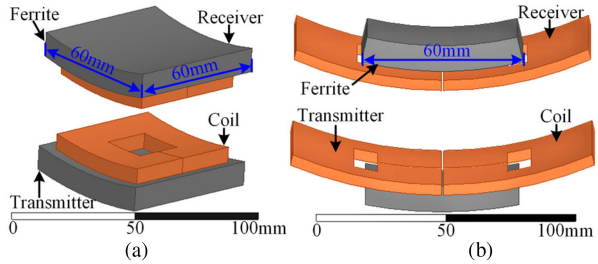

Fig. 21. (a) Nonpolarized arc circular MC. (b) Curly DD-DD bipolar MC.

TABLE III
Parameters of Actual MC

Parameters	Value	Parameters	Value
W_1	50 mm	W_3	60 mm
G	2°	W_4	60 mm
W_2	48 mm	Turns of transmitting coil 1	16
H_1	24 mm	Turns of transmitting coil 2	16
L_1	60 mm	Turns of receiving coil	20

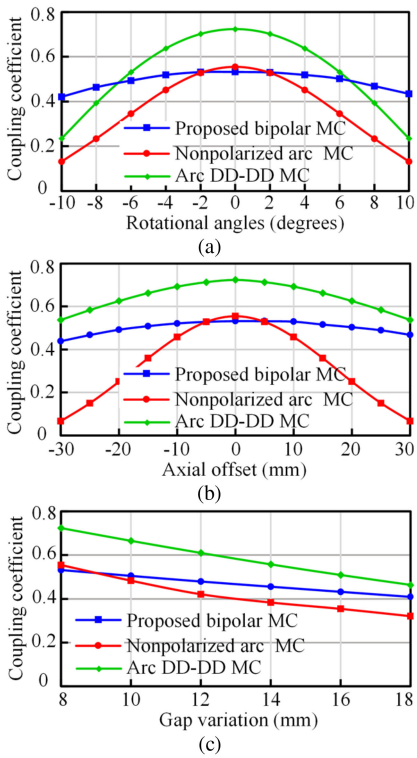

Fig. 22. Comparison of coupling coefficient k in the proposed MC with that in the previous nonpolarized arc circular MC and curly dc–dc MC over (a) rotational misalignment, (b) axial misalignment, and (c) gap variations.

A. Misaligned MC Combinations

Fig. 22 compares k in the proposed MC (by actual measurement) with that in the previous nonpolarized arc circular MC and curly DD-to-DD bipolar MC (by simulation, it is shown in Fig. 21). The comparison is carried out from three aspects: rotational misalignment, axial misalignment, and gap variations. Receiver weight is an important index to evaluate

TABLE IV
PARAMETERS OF THE PROTOTYPE SYSTEM

Parameters	Value	Parameters	Value
f	50kHz	L_1	37.5μH
L_P	102.4μH	C_P	272nF
L_S	69.47μH	C_1	156 nF
k	0.534	C_S	154nF

the performance of an AUV wireless charging system, so the ferrites of the unipolar arc circular receiver and DD receiver are set to be the same size as the proposed MC's receiver for a fair comparison.

Fig. 22(a) shows that k varies with rotational misalignment. It shows that as the rotational angle increases from –2° to 2°, the k in the arc circular MC is competitive or exceeds that of the proposed MC. However, as the rotational angle exceeds 2° (which ranges from –10° to –2° and 2° to 10°), the k of the nonpolarized arc circular MC drops dramatically and ends at 0.13; its variation is 76% as rotation misalignment from 0° to 10°. While k in the proposed MC is more stable, the variation is only 18%. The variations of k for both axial misalignment and gap variations are shown in Fig. 22(b) and (c), respectively. Similarly, the phenomenon still exhibits in the previous nonpolarized arc circular MC that the k drops rapidly with the rotating and increase gap. In the proposed MC, the k drops by 17% when the axial misalignment is 30 mm, and drops by 23% when the gap increases to 18 mm. Under the condition of precise alignment, the curly DD-to-DD bipolar MC exhibits strong coupling ability, the k is 0.72. However, its k drops dramatically with the rotational misalignments; k variation is 68% as rotation misalignment from 0° to 10°. In comparison, the proposed MC has a good tolerance to each dimension misalignment.

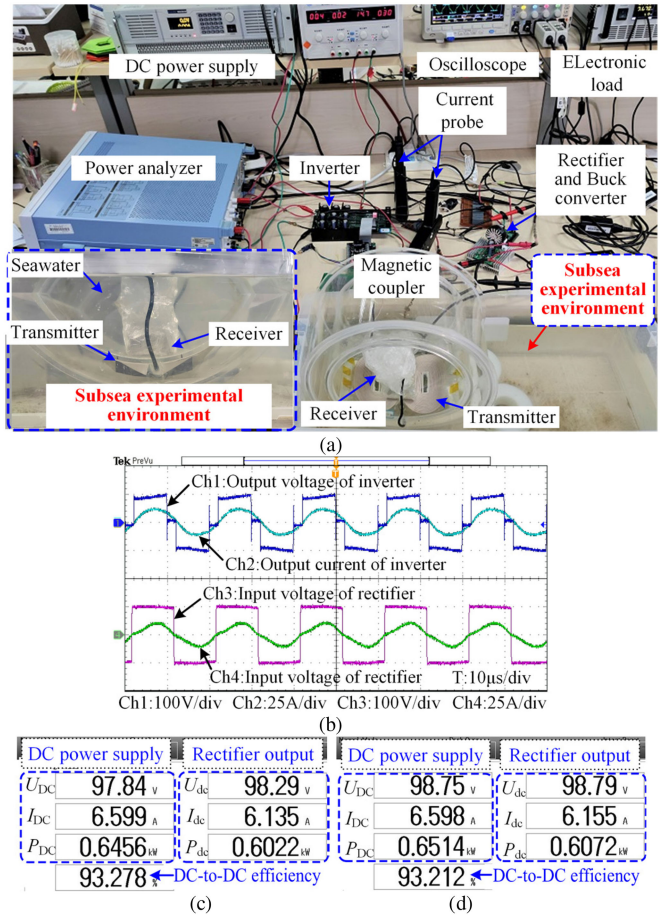

Fig. 23. (a) Power transfer experimental setup. (b) Waveforms of inverter output and rectifier input. (c) Power and efficiency test at $R_{dc} = 15.8\ \Omega$ in air condition. (d) Power and efficiency test at $R_{dc} = 15.8\ \Omega$ in seawater condition.

B. Power Transfer Capability

In order to determine the performance of the proposed MC, an AUV wireless charging prototype is developed in Fig. 23(a). The parameters of the prototype are given in Table IV. The power supply was fed by 100 V dc source, and was inverted to 50 kHz exciting current by inverter. The eddy current loss in seawater is directly related to the frequency, and the higher the frequency, the greater the loss [28]. Therefore, this article selects the lower working frequency of 50 kHz. Fig. 23(b) shows the waveforms of the inverter output and rectifier input. The output current of the inverter is slightly lagging the output voltage for achieving zero voltage switch (ZVS). It is worth mentioning that the influence of shielding aluminum shell on the magnetic field is involved in the later analysis, but the aluminum shell aluminum plate has no obvious effect on power transmission in a test, and it is not convenient for underwater test after adding aluminum shell, so the aluminum shell is only studied in the simulation.

The designed system was tested in air and seawater environment, and the results are shown in Fig. 23(c) and (d), respectively. It shows that the power is effectively transferred to the pick-up. In addition, the transmission efficiency in seawater is only slightly lower than that in air, this is because when the frequency is low, the performance of wireless charging system under water is similar to that in air [5], [28]. But in order to ensure the authenticity and accuracy of the experiment, the simulations and experiments (except magnetic flux leakage measurement) in this article are completed in the real seawater medium.

For the purpose of evaluated stability of power transfer against misalignments, the variations of output voltage U_{dc} with rotational misalignment, axial misalignment, and gap variation are measured, as shown in Fig. 24. Its performance was compared with the theoretical calculation by (12). In order to weaken the influence caused by voltage-division of the parasitic resistance, R_{dc} is selected as 100 Ω. From Fig. 24(a), it can be seen that U_{dc} decreases gradually with the increase of rotational degree, and the minimum value of U_{dc} is 80.8 V when the rolling angle is 10°. U_{dc} also decreases gradually due to axial misalignment and gap variation, and the minimum values of U_{dc} are 82.8 and 75 V, respectively. Above all, U_{dc} varies from 75 to 111.8 V. For lithium batteries with a nominal voltage of 48 V, the corresponding charging voltage at the CV stage should be 54 V, and the duty cycle of buck power controller ranges from 0.748 to 0.72, which is an effective condition for buck controller to charge the AUV.

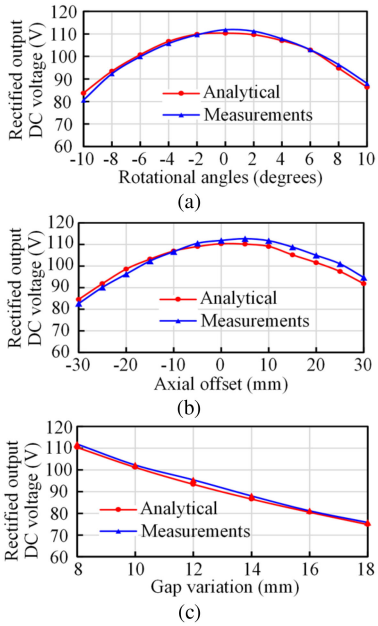

Fig. 24. Pick-up output dc voltage $U_{\rm dc}$ at $R_{\rm dc} = 100\ \Omega$ with (a) rotational misalignment, (b) axial misalignment, and (c) gap variations.

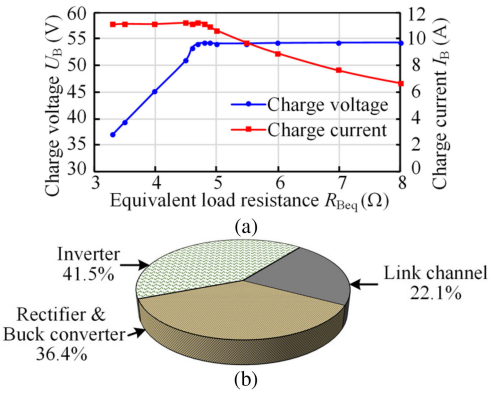

Fig. 25. (a) Charge voltage and charge current test of charging process. (b) System losses analysis.

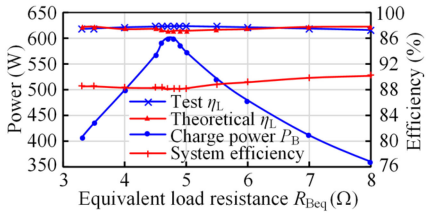

Fig. 26. Link efficiency $\eta_{\rm L}$, charge power $P_{\rm B}$, and overall system efficiency test.

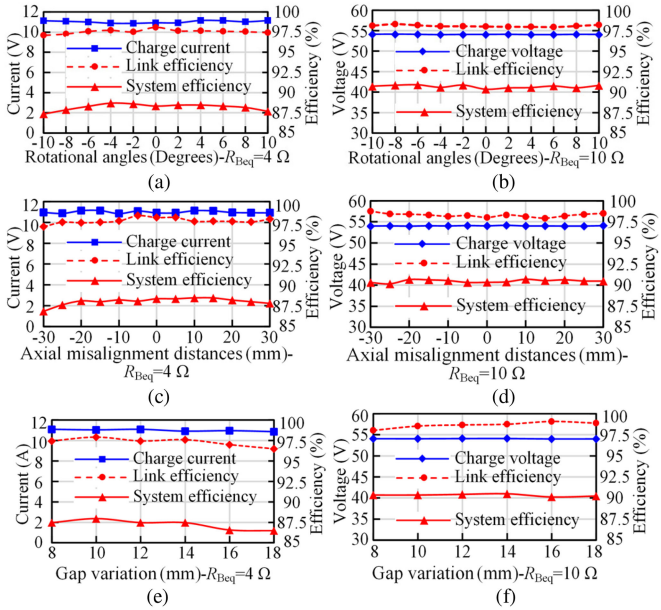

Fig. 27. (a) Charge current and efficiency variation with rotational angles at $R_{\rm Beq} = 4\ \Omega$. (b) Charge voltage and efficiency variation with rotational angles at $R_{\rm Beq} = 10\ \Omega$. (c) Charge current and efficiency variation with axial misalignment distances at $R_{\rm Beq} = 4\ \Omega$. (d) Charge voltage and efficiency variation with axial misalignment distances at $R_{\rm Beq} = 10\ \Omega$. (e) Charge current and efficiency variation with gap variation at $R_{\rm Beq} = 4\ \Omega$. (f) Charge voltage and efficiency variation with gap variation at $R_{\rm Beq} = 10\ \Omega$.

C. CC/CV Charging Test

The output charge voltage $U_{\rm B}$ and charge current $I_{\rm B}$ of the designed wireless charging system vary with $R_{\rm Beq}$, as shown in Fig. 25(a). It is found that $I_{\rm B}$ can be stable at 11 A in the CC charging stage and $U_{\rm B}$ can be stable at 54 V in the CV charging stage, and the switching between CC charging stage and CV charging stage can be realized normally. The system can achieve wireless charging function. The power loss distribution of the system is shown in Fig. 25(b). The losses of inverter, link channel and rectifier, and buck converter accounted for 41.5%, 22.1%, and 36.4% of the total losses, respectively.

Power analyzer is used to test the change of charge power $P_{\rm B}$, link efficiency $\eta_{\rm L}$, and overall system efficiency with the $R_{\rm Beq}$ during charging, as shown in Fig. 26. It can be seen that the theoretical value of link efficiency is close to the measured value. During the charging process, the high-power section coincides with the peak area of link efficiency, and the link-efficiency curve does shift to the left after efficiency optimization design. The overall system efficiency is higher than 88% and the link efficiency is higher than 97% in the charge power section of 350 W and above in the charging process. The maximum charging power is 599.3 W, and the maximum efficiency of the overall system is 90.6%.

Experiment studies on rotational, axial misalignment, and gap variation are conducted for the developed wireless charging system. The variations in charging current, charging voltage, link efficiency, and overall system efficiency for the system are shown in Fig. 27. In the above analysis, it is known that the $R_{\rm Beq}$ is 4 Ω corresponding to the CC charge stage and 10 Ω corresponding to the CV charge stage, and the misalignment performance is tested with these two load points, respectively. As the rotational angle increases from –10° to 10°, the charge current and charge voltage can be constant at 10 A and 54 V, respectively. Meanwhile, the link efficiency and overall system efficiency are relatively stable.

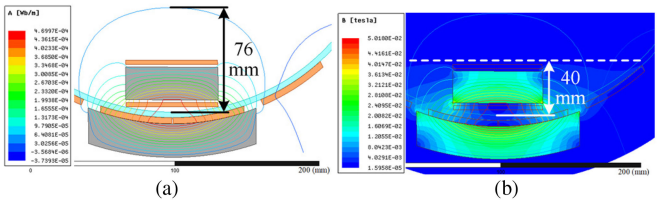

Fig. 28. Peak magnetic field distribution. (a) Flux lines and (b) magnetic flux densities on a cross section of the proposed MC.

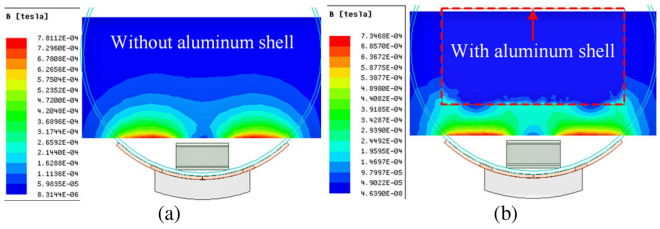

Fig. 29. Magnetic field distribution (a) without aluminum shell and (b) with aluminum shell.

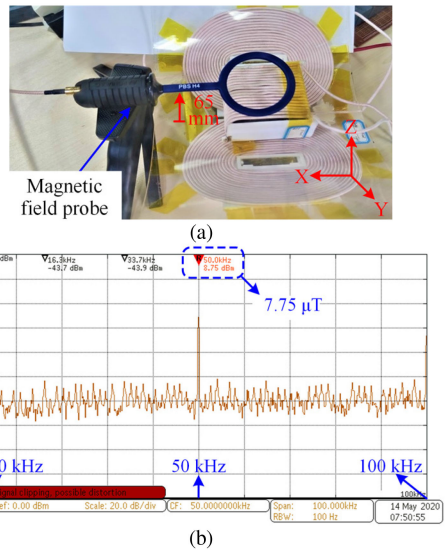

Fig. 30. (a) Experimental configuration for measuring Z-axis component of magnetic flux density B_Z. (b) Measured B_Z in 0 Hz $\leq f \leq$ 100 kHz.

As the axial misalignment distances increase from –30 to 30 mm and gap changes from 8 to 18 mm, the charge current, charge voltage link efficiency, and overall system efficiency also show excellent stability.

D. Magnetic Field Distribution

The magnetic field distribution is simulated as shown in Fig. 28, in which the number of amp-turns (NI) of per transmitting coil is 188 A·N since the number of turns of the per transmitting coil is 16 and the effective value of excitation current is 8.31 A at 600 W. Fig. 28(a) shows the distribution of the magnetic flux lines of the proposed MC. It can be found that most of the magnetic flux lines pass through the receiving coil, and only a small number of flux lines appear above the receiver. The magnet flux is guided by the receiving core to pass through the receiving coil. The magnetic field distribution of the proposed MC is further plotted as shown in Fig. 28(b). It shows that the alternating magnetic field is converged to the abdomen of the AUV. Especially in the area below 40 mm, the magnetic flux is concentrated within the magnetic structure itself. Therefore, the proposed MC has an excellent magnetic flux constraints capability, which improves the electromagnetic security of the wireless charging system.

Even though the proposed coil structure can suppress the magnetic field below the AUV's battery to some extent, to ensure safety, magnetic shielding remains indispensable. In fact, the AUV's battery is wrapped by a pressure-resistant aluminum alloy shell, which naturally forms a good magnetic leakage protection. As shown in Fig. 29, with the aluminum shell, the magnet field in the AUV is largely reduced. It is also found in the simulation that since the aluminum shell does not invade the strong magnetic field area, it hardly affects the self-inductance and mutual-inductance values, and only small eddy current loss is produced in practical application.

As shown in Fig. 30, the leakage flux was measured at the same point (25 mm from the center of the receiver along the Z axes), when the output power is approximately 600 W. Fig. 30(a) shows the placement of an AARONIA AG 1∗50 mm magnetic field probe relative to measuring Z-axis component of magnetic flux density B_Z. The shielding aluminum shell was not included in the leakage flux test. The B_Z measured at the field point is shown in Fig. 29(b). In the 0 Hz–100 kHz band, $B_Z \leq 7.75\ \mu$T. Similarly, a magnetic field probe is placed perpendicular to the X-axis and Y-axis, respectively, the X-axis component of magnetic flux density B_X and Y-axis component of magnetic flux density B_Y are obtained, $B_X \leq 7.20\ \mu$T, and $B_Y \leq 8.43\ \mu$T. According to guideline [29] and the test data of previous coil structures in [5], [15], and [16], it can be seen that the designed wireless charging system has low magnetic flux leakage.

E. Power Interoperability Study of the Developed Wireless Charging System

Considering the fact that AUVs of different power levels share the same underwater wireless charging base station, power interoperability should also be an important feature of the AUV wireless charging system. Since it is easy for a high-power system to be compatible with low-power charging, only the maximum power upper limit supported by the designed system is explored in this study.

By increasing the conduction angle of the inverter and reducing the load resistance, the output power of the system is increased by 1 kW, as shown in Fig. 31, and the corresponding dc–dc efficiency is 95.1%. Therefore, the designed underwater wireless charging system is capable of 1 kW wireless charging. After the AUV docking into the charging base station, it will make a request/response handshake with the charging base station. After knowing the power level of the charged AUV, the

TABLE V
COMPARISON WITH PREVIOUS AUV WIRELESS CHARGING SYSTEM

References	Cone type [12]	Coaxial ring type [16]	Three phase ring type [5]	Curly coil type [15]	This paper
Magnetic structure	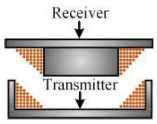	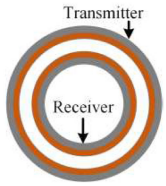	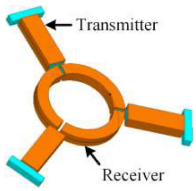	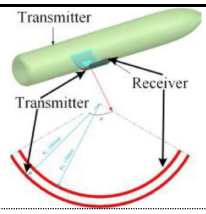	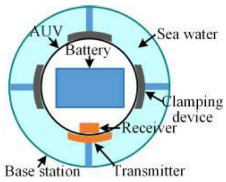
CC/CV charging	No	Yes	No	No	Yes
Power	500W	300W	1 kW	1 kW	1 kW
Maximum efficiency	96% (Coupling efficiency)	77% (DC-Battery efficiency)	92.41% (DC-DC efficiency)	95% (DC-DC efficiency)	95.1% (DC-DC efficiency)
The receiver occupies the radian of AUV hull	About 23°	360°	360°	60°	About 23°
Change AUV shape	Yes	No	No	No	No
Compact of receiver (Weight & Volume)	★★★★★	★★☆☆☆	★★☆☆☆	★★★★★	★★★★★
Easy to manufacture	★★★☆☆	★★★☆☆	★★★☆☆	★★★★☆	★★★★★
Easy to install at the AUV	★★☆☆☆	★★☆☆☆	★★★★☆	★★★★★	★★★★★
Compatibility of AUV with different diameters	★★☆☆☆	★★☆☆☆	★★★★★	★★★☆☆	★★★★★

A higher "⋆" represents better performance on this item, ⋆⋆⋆⋆⋆ means best.

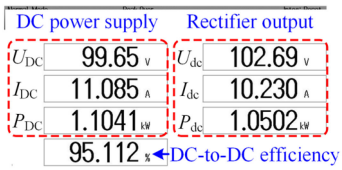

Fig. 31. Test results of output power improvement.

charging base station adjusts the conduction angle to meet the multipower compatibility.

F. Comparison With Previous AUV Wireless Charging System

In recent years, different inductive power transfers for AUV wireless charging have been reported. Sufficient power, high efficiency, high adaptability to AUV structure, small size, high misalignment tolerance, and low leakage magnetic field are indicators that should be considered comprehensively. A fair comparison of the typical AUV wireless charging systems is obtained, as shown in Table V, so that the optimal proposal can be chosen and applied. The proposal in this article is more lightweight and easier to install without changing the AUV shape. In conclusion, the scheme proposed in this article has strong practicability.

VI. CONCLUSION

In this article, a novel cross-coupling mode MC for AUV wireless charging systems is proposed. The arc bipolar transmitter can concentrate magnetic flux efficiently, and the dipole-coil-based receiver is employed to capture the horizontal magnetic flux. The magnetic flux of the proposed MC is investigated via the numerical simulation, which has shown that the chosen MC design has a good convergence effect of the magnetic field. To verify the effectiveness of the MC, a practical prototype is developed and analyzed. It shows that the developed system can successfully recharge the AUV with an 11 A constant current/54 V constant voltage charging mode. Besides, the proposal also has the good interoperability of AUVs with different diameters and different power levels, the system also can deliver 1.05 kW to an AUV with a dc–dc efficiency of 95.1%.

REFERENCES

[1] M. Carreras, J. D. Hernández, E. Vidal, N. Palomeras, D. Ribas, and P. Ridao, "Sparus II AUV—A hovering vehicle for seabed inspection," *IEEE J. Ocean. Eng.*, vol. 43, no. 2, pp. 344–355, Apr. 2018.

[2] C. C. Eriksen *et al.*, "Seaglider: A long-range autonomous underwater vehicle for oceanographic research," *IEEE J. Ocean. Eng.*, vol. 26, no. 4, pp. 424–436, Oct. 2001.

[3] M. Grasmueck *et al.*, "Autonomous underwater vehicle (AUV) mapping reveals coral mound distribution, morphology, and oceanography in deep water of the Straits of Florida," *Geophys. Res. Lett.*, vol. 33, no. 23, pp. 1–6, 2006.

[4] N. Palomeras, M. Carreras, P. Ridao, and E. Hernandez, "Mission control system for dam inspection with an AUV," in *Proc. IEEE/RSJ Int. Conf. Intell. Robots Syst.*, Beijing, China, 2006, pp. 2551–2556.

[5] T. Kan, R. Mai, P. P. Mercier, and C. C. Mi, "Design and analysis of a three-phase wireless charging system for lightweight autonomous underwater vehicles," *IEEE Trans. Power Electron.*, vol. 33, no. 8, pp. 6622–6632, Aug. 2018.
[6] A. M. Bradley, M. D. Feezor, H. Singh, and F. Y. Sorrell, "Power systems for autonomous underwater vehicles," *IEEE J. Ocean. Eng.*, vol. 26, no. 4, pp. 526–538, Oct. 2001.
[7] T. Orekan, P. Zhang, and C. Shih, "Analysis, design, and maximum power-efficiency tracking for undersea wireless power transfer," *IEEE J. Emerg. Sel. Topics Power Electron.*, vol. 6, no. 2, pp. 843–854, Jun. 2018.
[8] S. Huang, T. Lee, W. Li, and R. Chen, "Modular on-road AGV wireless charging systems via interoperable power adjustment," *IEEE Trans. Ind. Electron.*, vol. 66, no. 8, pp. 5918–5928, Aug. 2019.
[9] N. Khan, H. Matsumoto, and O. Trescases, "Wireless electric vehicle charger with electromagnetic coil-based position correction using impedance and resonant frequency detection," *IEEE Trans. Power Electron.*, vol. 35, no. 8, pp. 7873–7883, Aug. 2020.
[10] G. A. Covic and J. T. Boys, "Modern trends in inductive power transfer for transportation applications," *IEEE J. Emerg. Sel. Topics Power Electron.*, vol. 1, no. 1, pp. 28–41, Mar. 2013.
[11] C. Cai, S. Wu, L. Jiang, Z. Zhang, and S. Yang, "A 500-W wireless charging system with lightweight pick-up for unmanned aerial vehicles," *IEEE Trans. Power Electron.*, vol. 35, no. 8, pp. 7721–7724, Aug. 2020.
[12] T. Kojiya, F. Sato, H. Matsuki, and T. Sato, "Automatic power supply system to underwater vehicles utilizing non-contacting technology," in *Proc. Oceans MTS/IEEE Techno-Ocean*, Kobe, Japan, 2004, vol. 4, pp. 2341–2345.
[13] Z. Jie, D. J. Li, and C. Ying, "Frequency selection of an inductive contactless power transmission system for ocean observing," *Ocean Eng.*, vol. 60, pp. 175–185, 2013.
[14] C. Cai, Z. Yang, M. Qin, and S. Wu, "High transmission capacity P.U.A. wireless power transfer for AUV using an optimized magnetic coupler," in *Proc. IEEE Int. Magn. Conf.*, Singapore, 2018, p. 1.
[15] Z. Yan, Y. Zhang, K. Zhang, B. Song, and C. Mi, "Underwater wireless power transfer system with a curly coil structure for AUVs," *IET Power Electron.*, vol. 12, no. 10, pp. 2559–2565, 2019.
[16] M. Lin, D. Li, and C. Yang, "Design of an ICPT system for battery charging applied to underwater docking systems," *Ocean Eng.*, vol. 145, pp. 373–381, 2017.
[17] Z. Cheng, Y. Lei, K. Song, and C. Zhu, "Design and loss analysis of loosely coupled transformer for an underwater high-power inductive power transfer system," *IEEE Trans. Magn.*, vol. 51, no. 7, Jul. 2015, Art. no. 8401110.
[18] B. Song, Y. Wang, and K. Zhang," Research on wireless power transfer system for torpedo autonomous underwater vehicles," *Adv. Mech. Eng.*, vol. 10, no. 9, pp. 1–8, Aug. 2018.
[19] T. Assaf, C. Stefanini, and P. Dario, "Autonomous underwater biorobots: A wireless system for power transfer," *IEEE Robot. Autom. Mag.*, vol. 20, no. 3, pp. 26–32, Sep. 2013.
[20] Z. Yan, B. Song, Y. Zhang, K. Zhang, Z. Mao, and Y. Hu, "A rotation-free wireless power transfer system with stable output power and efficiency for autonomous underwater vehicles," *IEEE Trans. Power Electron.*, vol. 34, no. 5, pp. 4005–4008, May 2019.
[21] Z. Li *et al.*, "Design considerations for electromagnetic couplers in contactless power transmission systems for deep-sea applications," *J. Zhejiang Univ. Sci. C*, vol. 11, no. 20, pp. 824–834, 2010.
[22] S. Li and C. C. Mi, "Wireless power transfer for electric vehicle applications," *IEEE J. Emerg. Sel. Topics Power Electron.*, vol. 3, no. 1, pp. 4–17, Mar. 2015.
[23] M. Budhia, J. T. Boys, G. A. Covic, and C. Huang, "Development of a single-sided flux magnetic coupler for electric vehicle IPT charging systems," *IEEE Trans. Ind. Electron.*, vol. 60, no. 1, pp. 318–328, Jan. 2013.
[24] F. Y. Lin, C. Carretero, G. A. Covic, and J. T. Boys, "A reduced order model to determine the coupling factor between magnetic pads used in wireless power transfer," *IEEE Trans. Transp. Electrific.*, vol. 3, no. 2, pp. 321–331, Jun. 2017.
[25] T. Ressurreição *et al.*, "System design for wireless powering of AUVs," in *Proc. OCEANS*, Aberdeen, U.K., 2017, pp. 1–6.
[26] Z. Li, C. Zhu, J. Jiang, K. Song, and G. Wei, "A 3-kW wireless power transfer system for sightseeing car supercapacitor charge," *IEEE Trans. Power Electron.*, vol. 32, no. 5, pp. 3301–3316, May 2017.
[27] R. L. Steigerwald, "A comparison of half-bridge resonant converter topologies," *IEEE Trans. Power Electron.*, vol. 3, no. 2, pp. 174–182, Apr. 2002.
[28] Z. Yan *et al.*, "Frequency optimization of a loosely coupled underwater wireless power transfer system considering eddy current loss," *IEEE Trans. Ind. Electron.*, vol. 66, no. 5, pp. 3468–3476, May 2019.
[29] "Guidelines for limiting exposure to time-varying electric, magnetic, and electromagnetic fields (up to 300 GHz)," *Health Phys.*, vol. 74, no. 4, pp. 494–522, Dec. 1998.

Chunwei Cai was born in Shandong, China, in 1977. He received the B.S. and M.S. degrees in control theory and control engineering from Shandong University, Jinan, China, in 2001 and 2004, respectively, and the Ph.D. degree in electrical engineering from the Harbin Institute of Technology (HIT), Harbin, China, in 2013.

In 2006, he was a Lecturer with the HIT, Weihai, China, where he has been an Assistant Professor since 2014. His research interests include wireless power transfer systems, power converters, and inverters.

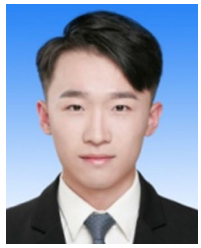

Shuai Wu received the B.S. degree in electrical engineering and automation from Shanxi Agricultural University, Jinzhong, China, in 2017, and the M.S. degree in electrical engineering, in 2019, from the Harbin Institute of Technology, Weihai, China, where he is currently working toward the Ph.D. degree.

His research interests include wireless power transfer for autonomous underwater vehicles and unmanned aerial vehicles.

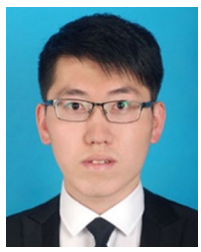

Zhipeng Zhang was born in Shanxi, China, in 1993. He received the B.S. degree in electrical engineering and automation from Yanshan University, Qinhuangdao, China, in 2016. He is currently working toward the M.S. degree in electrical engineering with the Academy of New Energy, Harbin Institute of Technology, Weihai, China.

His research interests include power electronics and wireless power transfer system for autonomous underwater vehicles.

Longyun Jiang was born in Shandong, China, in 1997. He received the B.S. degree in electrical engineering and automation from Qingdao University of Technology, Qingdao, China, in 2019. He is currently working toward the M.S. degree in electrical engineering with the Academy of New Energy, Harbin Institute of Technology, Weihai, China.

His research interests include power electronics and wireless power transfer system for unmanned aerial vehicle.

Shiyan Yang received the B.S. and M.S. degrees in electrical engineering and Ph.D. degree in welding engineering from the Harbin Institute of Technology, Harbin, China, in 1984, 1989, and 1998, respectively.

He is currently a Professor with the Department of Electrical Engineering, Harbin Institute of Technology. His research interests include high-power power supply and its application, energy storage system and its equilibrium, and fundamental theory of finite power supply drive and key commonsense problem.